

**Optimal Arrangements of 1,3-Diphenylisobenzofuran  
Molecule Pairs for Fast Singlet Fission**

Journal:	<i>Photochemical &amp; Photobiological Sciences</i>
Manuscript ID	PP-ART-07-2019-000283.R1
Article Type:	Paper
Date Submitted by the Author:	29-Jul-2019
Complete List of Authors:	Buchanan, Eric; University of Colorado at Boulder, Department of Chemistry Michl, Josef; University of Colorado at Boulder, Department of Chemistry; Academy of Sciences of the Czech Republic, Institute of Organic Chemistry and Biochemistry

## Optimal Arrangements of 1,3-Diphenylisobenzofuran Molecule Pairs for Fast Singlet Fission

Eric A. Buchanan<sup>†</sup> and Josef Michl<sup>‡¶</sup>

<sup>†</sup> *Department of Chemistry, University of Colorado, Boulder, CO 80309-0215, United States,*

<sup>¶</sup> *Institute of Organic Chemistry and Biochemistry, Academy of Sciences of the Czech Republic, Flemingovo nám. 2, 16610 Prague 6, Czech Republic*

**Abstract:** A simplified version of the frontier orbital model has been applied to pairs of  $C_2$ ,  $C_{2v}$ ,  $C_s$ , and  $C_1$  symmetry 1,3-diphenylisobenzofuran rotamers to determine their best packing for fast singlet fission (SF). For each rotamer the square of the electronic matrix element for SF was calculated at  $2.2 \times 10^9$  pair geometries and a few thousand most significant physically accessible local maxima were identified in the six-dimensional space of mutual arrangements. At these pair geometries, SF energy balance was evaluated, relative SF rate constants were approximated using Marcus theory, and the SF rate constant  $k_{\text{SF}}$  was maximized by further optimization of the geometry of the molecular pair. The process resulted in 142, 67, 214, and 291 unique geometries for the  $C_2$ ,  $C_{2v}$ ,  $C_s$ , and  $C_1$  symmetry molecular pairs, respectively, predicted to be superior to the  $C_2$  symmetrized known crystal pair structure. These optimized pair geometries and their triplet biexciton binding energies are reported as targets for crystal engineering and/or covalent dimer synthesis, and as possible starting points for high-level pair geometry optimizations.

## Introduction

Singlet fission (SF) is a photophysical process in a molecular solid in which a singlet exciton shares some of its energy with a nearby ground state chromophore to produce a singlet biexciton carrying two coupled triplet excitations, which then dissociates into two independent triplet excitons.<sup>1,2,3,4</sup> Despite the increased interest in SF since it was shown<sup>5</sup> to be capable of increasing the theoretical efficiency of single-junction solar cells beyond the Shockley-Queisser limit,<sup>6</sup> much remains unknown regarding how to best design efficient materials.

Practical SF solids should not only undergo SF fast enough to outcompete any potential loss pathways, producing a high triplet yield, but must also meet many additional requirements, such as photostability and environmental friendliness. Few if any are known to meet these conditions, and additional ones are sought in many laboratories. The search is both for finding suitable chromophores and for finding their best packing in the solid phase, known to affect triplet yields significantly.<sup>7,8,9,10,11,12,13,14,15,16</sup> Here we address the latter and identify those geometries of molecular pairs that maximize the rate constant for the formation of the singlet biexciton. At these geometries, we also calculate the biexciton binding energies. These results represent only the first step toward packing optimization for triplet yields, which would also require the evaluation of the rates of all competing decay channels.

We treat only pairs of chromophores at a time. This is adequate for studies of amorphous solids, of covalent dimers, and of SF in solutions, and is likely to provide general insight into the structural factors important in SF. For a prediction of desirable packing patterns in crystalline solids, both theory<sup>17,18,19,20,21</sup> and experiment<sup>22</sup> suggest that it will ultimately be necessary to consider the geometrical arrangements of a larger number of molecules simultaneously, but we do not do so now.

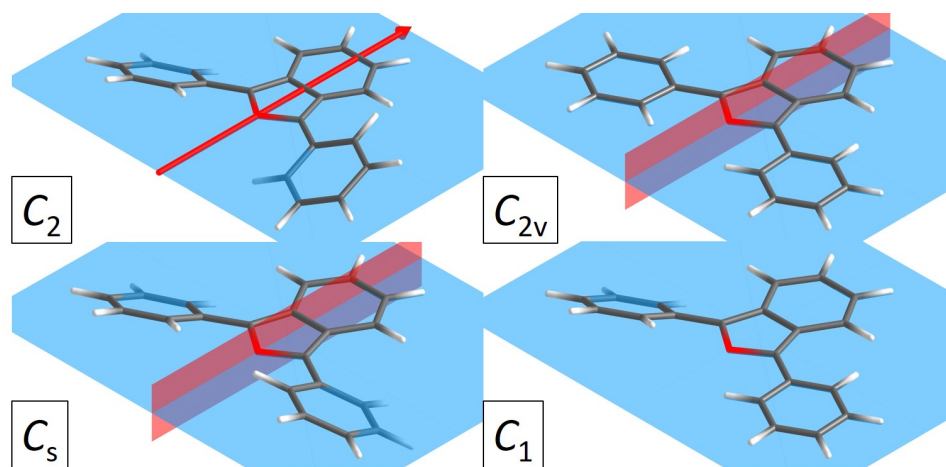


**Figure 1.**  $C_2$ ,  $C_{2v}$ ,  $C_s$ , and  $C_1$  rotamers of **1**. The  $xy$  plane of the isobenzofuran ring is shown in blue, the  $y$  axis of twofold symmetry in **1**( $C_2$ ) and the  $yz$  plane of symmetry in **1**( $C_{2v}$ ) and **1**( $C_s$ ) are shown in red.

The chromophore we have chosen to work with is 1,3-diphenylisobenzofuran (**1**).<sup>9,23,24,25,26,27</sup>

This is the first successful chromophore theoretically designed to approximately satisfy the requirement for isoergic SF<sup>28</sup> and its  $\alpha$  polymorph has a room-temperature triplet yield of  $140 \pm 25\%$ ,<sup>23,26</sup> which increases to  $200 \pm 30\%$  at 77 K. It thus is an ideal candidate for packing optimization to attempt to push its room-temperature triplet yield closer to 200%. Measurements on three variously fluorinated derivatives of **1** in thin films<sup>22</sup> followed by a more comprehensive study currently in progress<sup>29</sup> have indeed shown that crystal packing is decisive. Only about half of the compounds exhibit singlet fission, some faster than others, while the other half only form excimers. Up to now, it has however not been clear what packing to aim for to maximize the triplet yield.

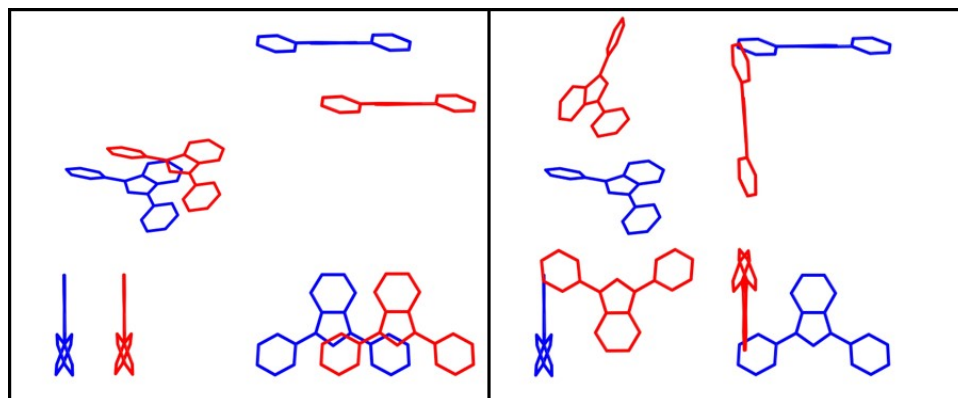


**Figure 2.** Multi-view projections of pair geometries found in the crystal structure of **1**( $C_2$ ). Left, a slip-stacked pair; right, a herringbone pair.

The crystal structure of **1** contains both herringbone and slip-stacked pair motifs (Figure 2) and attracts attention by its peculiar polymorphism: the  $\alpha$  and  $\beta$  forms have an almost identical crystal structure. All nearest-neighbor molecular pairs are effectively identical in the two forms, and only the relations between next-nearest neighbors are different.<sup>22</sup> Yet, the SF rate constant in the former is about 6 times larger than that in the latter. As a result, a pair model cannot differentiate between the two, but it might still suggest which type of structure to aim for.

Figure 1 shows the four rotamers of **1** that are investigated in this study. The phenyl groups in the  $C_2$  and  $C_s$  rotamers are disrotated and conrotated out of the plane of the isobenzofuran moiety, respectively, whereas in the  $C_{2v}$  rotamer both lie in this plane. In the  $C_1$  rotamer one phenyl group is in the plane and the other is rotated. These four rotamers reflect symmetrized chromophore geometries found in crystals of variously fluorinated derivatives of **1**.<sup>22</sup> Presently, the packing structure within pairs of each of the four rotamers will be optimized, keeping the same rigid structure for both partners in a pair.

Even in the presently adopted pair approximation, an exhaustive search on a modest grid for all feasible packing geometries of molecular pairs that are optimal for  $k_{\text{SF}}$  requires calculations at billions of geometries, precluding the use of highly accurate methods. Since we only wish to identify those approximate molecular pair geometries at which the function  $k_{\text{SF}}$  has local maxima and hope for qualitative insights, rather than seeking a quantitative prediction of absolute SF rates, the use of a simplified model<sup>30</sup> for  $\pi$ -electron chromophores appears to be reasonable.

The model works in a diabatic picture and starts with the Fermi Golden Rule, according to which the rate constant of SF is proportional to the squared electronic matrix element  $|T|^2$ , which we calculate, and to the Frank-Condon weighted density of states, whose effects we approximate using Marcus theory.<sup>31,32,33</sup> The calculation of  $|T|^2$  is based on a simplified frontier orbital treatment of intermolecular interactions, previously tested against high-level ab initio results.<sup>29,34</sup> We first scan the six-dimensional space of possible pair geometries to find the maxima of  $|T|^2$ , avoiding structures that are physically inaccessible due to molecular impenetrability. The six degrees of freedom are translations of partner B relative to A along the  $x$ ,  $y$ , and  $z$  axes and its rotation about them. A few thousand of the largest maxima are selected for further geometrical optimization to maximize  $k_{\text{SF}}$  calculated using Marcus theory. At each local maximum, the biexciton binding energy is also computed. The limitations of Marcus theory are known and the absolute rates predicted can be off by several orders of magnitude, but we are only interested in relative values.

We first briefly review the theory behind the model, which is described in detail elsewhere,<sup>35,36</sup> and then discuss the results of its application to **1**. Finally, we apply qualitative rules derived from first-order perturbation theory<sup>35,37</sup> to selected pair geometries to gain further understanding of the relationship between packing structure and the SF rate constant  $k_{\text{SF}}$ .

## Method

**(i) Scope.** The frontier orbital model has been used for molecular solids for decades.<sup>1,3,6,7,34,38,39</sup> It assumes that the lowest-lying electronic excited states can be described well in an active space comprised of only frontier orbitals: the highest occupied molecular orbital (HOMO) and the lowest unoccupied molecular orbital (LUMO). Here, it is applied to a pair of molecules, resulting in an active space of four electrons in four orbitals: the HOMOs ( $h_A, h_B$ ) and LUMOs ( $l_A, l_B$ ) of partners A and B in the pair. This leads to 20 singlet configurations, but we only include the five known to be most important to the SF process: two that are locally excited (LE) on one of the partners,  $|S_1S_0\rangle$  and  $|S_0S_1\rangle$ , two of charge-transfer (CT) nature,  $|^1D^+D^-\rangle$  and  $|^1D^-D^+\rangle$ , where an electron has been transferred from one partner to the other, and one of biexciton (BE) nature, where triplet excitations on each partner are coupled into an overall singlet,  $|^1T_1T_1\rangle$ . We assume that in the absence of intermolecular interactions, the two LE and one BE configurations would be of equal energy, whereas the two CT configurations would both be 2 eV higher as long as the partners touch. The measured  $S_1$  excitation energy of **1** is 2.8 eV in toluene solution, while the  $T_1$  excitation energy is 1.4 eV in a thin film of the solid<sup>27</sup> and 1.5 eV in benzene solution.<sup>40</sup> The energy of the CT configurations is a rough guess based on previous calculations for covalent dimers of **1**.<sup>41</sup>

**(ii) Approximations.** Molecular orbitals (MOs) are expanded in a valence basis set of natural atomic orbitals (NAOs). Zero differential overlap (ZDO)<sup>42</sup> is assumed and intermolecular overlap is neglected in the interaction Hamiltonian,  $H_{\text{int}}$ . Intermolecular matrix elements of the ground state Fock operator are approximated by  $F_{\mu\nu} = \alpha S_{\mu\nu}$ ,<sup>34,43,44,45</sup> where the proportionality factor  $\alpha = (\alpha_\mu + \alpha_\nu)/2$  is the average of the Extended Hückel theory Coulomb integrals (electron binding energy) of the valence  $p_z$  orbitals on atoms  $\mu$  and  $\nu$  and  $S_{\mu\nu}$  is their overlap.

**(iii) State Energies.** The two LE configurations are coupled through excitation energy transfer expressed in the two-electron integral  $2(h_A l_A | h_B l_B)$ , allowing them to produce in-phase ( $|S^+\rangle$ ) and out-of-phase ( $|S^-\rangle$ ) combinations. Within the ZDO approximation, there is no direct coupling between the LE configurations and the BE configuration. However, both are coupled to the CT states, allowing them to interact indirectly. This is known as the mediated or “superexchange” pathway, expressed in the matrix of the  $H_{\text{int}}$  operator:

$\hat{H}_{\text{int}}$	$ S_1 S_0\rangle$	$ S_0 S_1\rangle$	$ ^1D^+ D^-\rangle$	$ ^1D^- D^+\rangle$	$ ^1T_1 T_1\rangle$
$\langle S_1 S_0  $	$E(S_1 S_0)$	$2(h_A l_A   h_B l_B)$	$\langle l_A   \hat{F}   l_B \rangle$	$-\langle h_A   \hat{F}   h_B \rangle$	0
$\langle S_0 S_1  $	$2(h_A l_A   h_B l_B)$	$E(S_0 S_1)$	$-\langle h_A   \hat{F}   h_B \rangle$	$\langle l_A   \hat{F}   l_B \rangle$	0
$\langle ^1D^+ D^-  $	$\langle l_A   \hat{F}   l_B \rangle$	$-\langle h_A   \hat{F}   h_B \rangle$	$E(^1D^+ D^-)$	0	$(3/2)^{1/2} \langle l_A   \hat{F}   h_B \rangle$
$\langle ^1D^- D^+  $	$-\langle h_A   \hat{F}   h_B \rangle$	$\langle l_A   \hat{F}   l_B \rangle$	0	$E(^1D^- D^+)$	$(3/2)^{1/2} \langle h_A   \hat{F}   l_B \rangle$
$\langle ^1T_1 T_1  $	0	0	$(3/2)^{1/2} \langle l_A   \hat{F}   h_B \rangle$	$(3/2)^{1/2} \langle h_A   \hat{F}   l_B \rangle$	$E(^1T_1 T_1)$

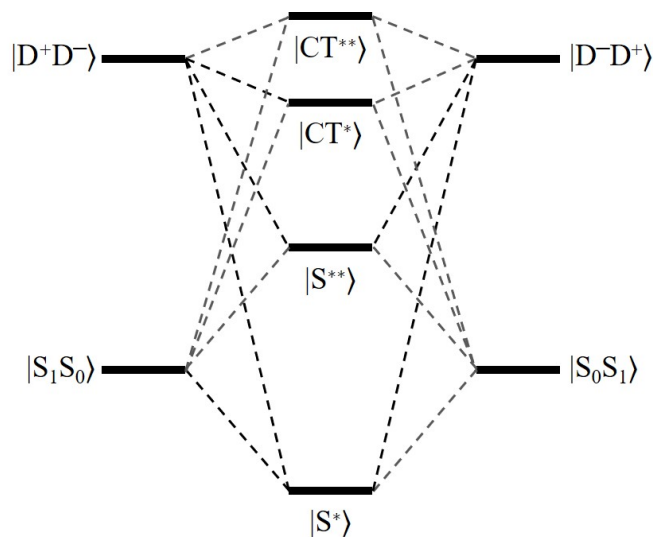


**Figure 3.** Energy level diagram of configurations (left and right) and the initial singlet states resulting from  $4 \times 4$  diagonalization (center).

The initial diabatic states are obtained by a  $4 \times 4$  diagonalization of the LE and CT configurations, which yields two excitonic states,  $|S^* \rangle$  at lower and  $|S^{**} \rangle$  at higher energy, plus two states of predominantly CT character (Figure 3). When the coupling between the LE and CT states is weak, it can be described by first-order perturbation theory, which leads to a particularly simple algebraic result. In this work, we will use the  $4 \times 4$  diagonalization ('Procedure III' in refs. 29 and 35). The two initial diabatic states then are  $|S^* \rangle$  and  $|S^{**} \rangle$ , and the final diabatic state is obtained by a  $3 \times 3$  diagonalization of the CT and BE configurations. The three states are symmetrically orthogonalized against each other and have the form:

$$|S^* \rangle = \lambda_{1,1}|S_1S_0 \rangle + \lambda_{1,2}|S_0S_1 \rangle + \lambda_{1,3}|D^+D^- \rangle + \lambda_{1,4}|D^-D^+ \rangle + \lambda_{1,5}|T_1T_1 \rangle \quad (1a)$$

$$|S^{**} \rangle = \lambda_{2,1}|S_1S_0 \rangle + \lambda_{2,2}^*|S_0S_1 \rangle + \lambda_{2,3}^*|D^+D^- \rangle + \lambda_{2,4}^*|D^-D^+ \rangle + \lambda_{2,5}^*|T_1T_1 \rangle \quad (1b)$$

$$|^1\text{TT}^*\rangle = \lambda_{3,1} * |S_1 S_0\rangle + \lambda_{3,2} * |S_0 S_1\rangle + \lambda_{3,3} * |^1\text{D}^+ \text{D}^-\rangle + \lambda_{3,4} * |^1\text{D}^- \text{D}^+\rangle + \lambda_{3,5} * |^1\text{T}_1 \text{T}_1\rangle \quad (1c)$$

**(iv) Marcus Theory SF Rate Constant.** The energies of the three diabatic states and the CT mediated couplings between the S\* and S\*\* states and final <sup>1</sup>TT\* state are next used to calculate the SF rate constant using eqs. (2). Two-level Boltzmann statistics<sup>46</sup> are used to average the SF rate constants for S\* and S\*\* according to eq. (3).

$$k(\text{S}^*) = (2\pi/\hbar) |T^*|^2 (4\pi\lambda k_B T)^{-1/2} \exp[-(\Delta E_{\text{SF}}(\text{S}^*) + \lambda)^2 / 4\pi\lambda k_B T] \quad (2a)$$

$$k(\text{S}^{**}) = (2\pi/\hbar) |T^{**}|^2 (4\pi\lambda k_B T)^{-1/2} \exp[-(\Delta E_{\text{SF}}(\text{S}^{**}) + \lambda)^2 / 4\pi\lambda k_B T] \quad (2b)$$

$$k(\text{SF}) = \{1 - [\exp(-\Delta E_{\text{DS}}/k_B T) + 1]^{-1}\} k(\text{S}^*) + \{[\exp(-\Delta E_{\text{DS}}/k_B T) + 1]^{-1}\} k(\text{S}^{**}) \quad (3)$$

$T^*$  and  $T^{**}$  are the SF couplings between the S\* or S\*\* and <sup>1</sup>TT\* states, respectively, and  $\Delta E_{\text{SF}}$  is their energy difference while  $\Delta E_{\text{DS}}$  is the Davydov splitting,  $\Delta E(\text{S}^{**}) - \Delta E(\text{S}^*)$ . Reorganization energy  $\lambda$  is calculated from  $\lambda = E[\text{T}_1, q(\text{S}_1)] + E[\text{T}_1, q(\text{S}_0)] - 2 \times E[\text{T}_1, q(\text{T}_1)]$ .<sup>47</sup> Here  $q$  denotes the equilibrium geometry of the isolated molecule in the designated state.

**(v) Qualitative Design Rules.** To gain insight into the structural features which enhance SF, we will analyze a few optimized pair geometries with previously published<sup>35,36</sup> design rules derived by first-order perturbation theory, eqs. (4). Orbitals  $p$  and  $q$  are the semi-localized orbitals  $p = 2^{-1/2}(h + l)$  and  $q = 2^{-1/2}(h - l)$ , where  $h$  and  $l$  are the HOMO and LUMO. In the overlap integral  $S_{\mu\nu}$ , the first index refers to an atomic orbital on partner A and the second, on partner B. The two-electron integral  $2(h_A l_A | h_B l_B)$  is typically the most significant contributor to the Davydov splitting and

upon transformation to the  $p$  and  $q$  basis it is the sum and difference of Coulomb interactions between semi-localized charge densities.

$$|T^+| \propto |(S_{hh} - S_{ll})(S_{hl} + S_{lh})| = |(S_{pp} - S_{qq})(S_{pq} + S_{qp})| \quad (4a)$$

$$|T^-| \propto |(S_{hh} + S_{ll})(S_{hl} - S_{lh})| = |(S_{pp} + S_{qq})(S_{qp} - S_{pq})| \quad (4b)$$

$$(h_A l_A | h_B l_B) = (1/4) \{ (p_A p_A | p_B p_B) - (p_A p_A | q_B q_B) - (q_A q_A | p_B p_B) + (q_A q_A | q_B q_B) \} \quad (4c)$$

$$\begin{aligned} \Delta E_{DS} = \Delta E(S^+) - \Delta E(S^-) = (1/2) [2 \{ (p_A p_A | p_B p_B) - (p_A p_A | q_B q_B) - (q_A q_A | p_B p_B) + (q_A q_A | q_B q_B) \} + \\ (S_{pp} + S_{qq})^2 - (S_{pq} + S_{qp})^2] \end{aligned} \quad (4d)$$

$$\begin{aligned} \Delta E_{SF}(S^+) = (-1/4) (2 \{ (p_A p_A | p_B p_B) - (p_A p_A | q_B q_B) - (q_A q_A | p_B p_B) + (q_A q_A | q_B q_B) \} + (1/2) [3 \{ S_{pp} - S_{qq} \}^2 - \\ \{ S_{pq} + S_{qp} \}^2 - 5 \{ S_{pq} \times S_{qp} \}]) \end{aligned} \quad (4e)$$

$$\begin{aligned} \Delta E_{SF}(S^-) = (1/4) (2 \{ (p_A p_A | p_B p_B) - (p_A p_A | q_B q_B) - (q_A q_A | p_B p_B) + (q_A q_A | q_B q_B) \} - (1/2) [3 \{ S_{pq} - S_{qp} \}^2 - \\ \{ S_{pp} + S_{qq} \}^2 - 5 \{ S_{pp} \times S_{qq} \}]) \end{aligned} \quad (4f)$$

**Computational Procedures.** Geometries used to calculate reorganization energy were optimized in ORCA<sup>48</sup> using DFT for the  $S_0$  and  $T_1$  electronic states and TD-DFT (TDA<sup>49</sup>) for the  $S_1$  electronic state using the PBE0<sup>50</sup> functional with the Def2-TZVP<sup>51</sup> basis set and the RIJCOSX<sup>52,53</sup> approximation for Coulomb and exchange integral evaluation with Def2/JK.<sup>54</sup> The Def2-TZVPD<sup>50,55</sup> basis and auxiliary basis set generated by the AUTOAUX<sup>56</sup> procedure were used for single point energy evaluations with analytic integral evaluation. Singlet excitation energies were calculated via TD-DFT<sup>57</sup> without the TDA. Triplet energies were calculated using the  $\Delta$ SCF<sup>58</sup> method. Frequency analysis was performed on all optimized geometries to ensure they were true minima. The SIMPLE

program<sup>29,35</sup> was used to calculate all singlet fission couplings, excitonic contributions to energetics, and Marcus theory rates.

**SIMPLE<sup>29,35</sup> Procedure Details.** The crystal structure of **1** was symmetrized to  $C_2$ ,  $C_{2v}$ , and  $C_s$  point symmetry groups, yielding three of the rotamers. The  $C_1$  rotamer geometry was generated from those of the  $C_{2v}$  and  $C_2$  rotamers. The quantum chemistry program ORCA<sup>47</sup> version 4.0.1 was used to calculate MOs with the RHF<sup>59</sup> method using the 6-311G<sup>60</sup> basis set. Natural bonding orbital (NBO) analysis was performed by the NBO 6.0 program<sup>61</sup> linked to ORCA to generate NAOs. Since the  $C_{2v}$  rotamer has  $xy$  and  $yz$  planes of symmetry (Fig. 1), only one quadrant of the translational space is unique. Chromophore B was therefore translated relative to A in 0.5 Å increments along the positive  $x$  axis for 32 steps, the positive  $z$  axis for 22 steps, and both the positive and negative  $y$  axis for 25 steps. It was rotated about its  $x$ ,  $y$ , and  $z$  axes for 25 steps of +15° increments, resulting in  $5.5 \times 10^8$  pair geometries. The  $C_2$  rotamer's reduced symmetry requires additional translational steps along the negative  $x$  axis while the  $C_s$  rotamer's reduced symmetry requires them along the negative  $z$  axis, resulting in  $1.1 \times 10^9$  pair geometries each. As the  $C_1$  rotamer does not benefit from any symmetry, it requires translational steps in the positive and negative direction for all three axes, resulting in  $2.2 \times 10^9$  pair geometries.

The 2,016, 1,276, 2,754, and 4,396 physically accessible geometries with the largest SF coupling squared for the  $C_2$ ,  $C_{2v}$ ,  $C_s$ , and  $C_1$  rotamers, respectively, were selected for optimization for maximum  $k_{\text{SF}}$ . The reorganization energy of the  $C_2$  rotamer was calculated to be 400 meV and was used for rate constant calculations for all rotamers. The optimizations resulted in 142, 67, 214, and 291 unique geometries for the  $C_2$ ,  $C_{2v}$ ,  $C_s$ , and  $C_1$  rotamers, respectively, which were predicted to be improvements over or equivalent to the  $C_2$  symmetrized crystal slip-stacked pair structure.

When the energy balance without intermolecular interaction was increased from zero to 100 meV and the  $C_{2v}$  pair geometries were re-optimized, the structures remained essentially unchanged. The rate constants however were all depressed by about an order of magnitude due to the increased endothermicity and in regions where rate constants of different pair geometries did not differ by much, the order of some pairs exchanged.

## Results

Multi-view projections of the first five optimized pair geometries for the four rotamers of **1** are shown in Figure 4 and the next five are shown in Figure 5. Pairs 11 through 30 for the  $C_{2v}$  rotamer are shown in Figure 6. The multi-view projections follow the standard third-angle projection method: the main view of the  $xy$  plane is located in the lower right, the top view of the  $xz$  plane is above that and is the view if the main view were rotated  $90^\circ$  about the  $x$  axis out of the plane of the page from the top to bottom, the left side view of the  $yz$  plane is to the left and is the view if the main view were rotated  $90^\circ$  about the  $y$  axis out of the plane of the page from the left to right. Energy values, couplings, and ratios of the predicted SF rate constants to that of the slip-stacked pair in the crystal ( $k_0 = 1.05 \times 10^8 \text{ s}^{-1}$ ) are provided in Tables 1 and 2.

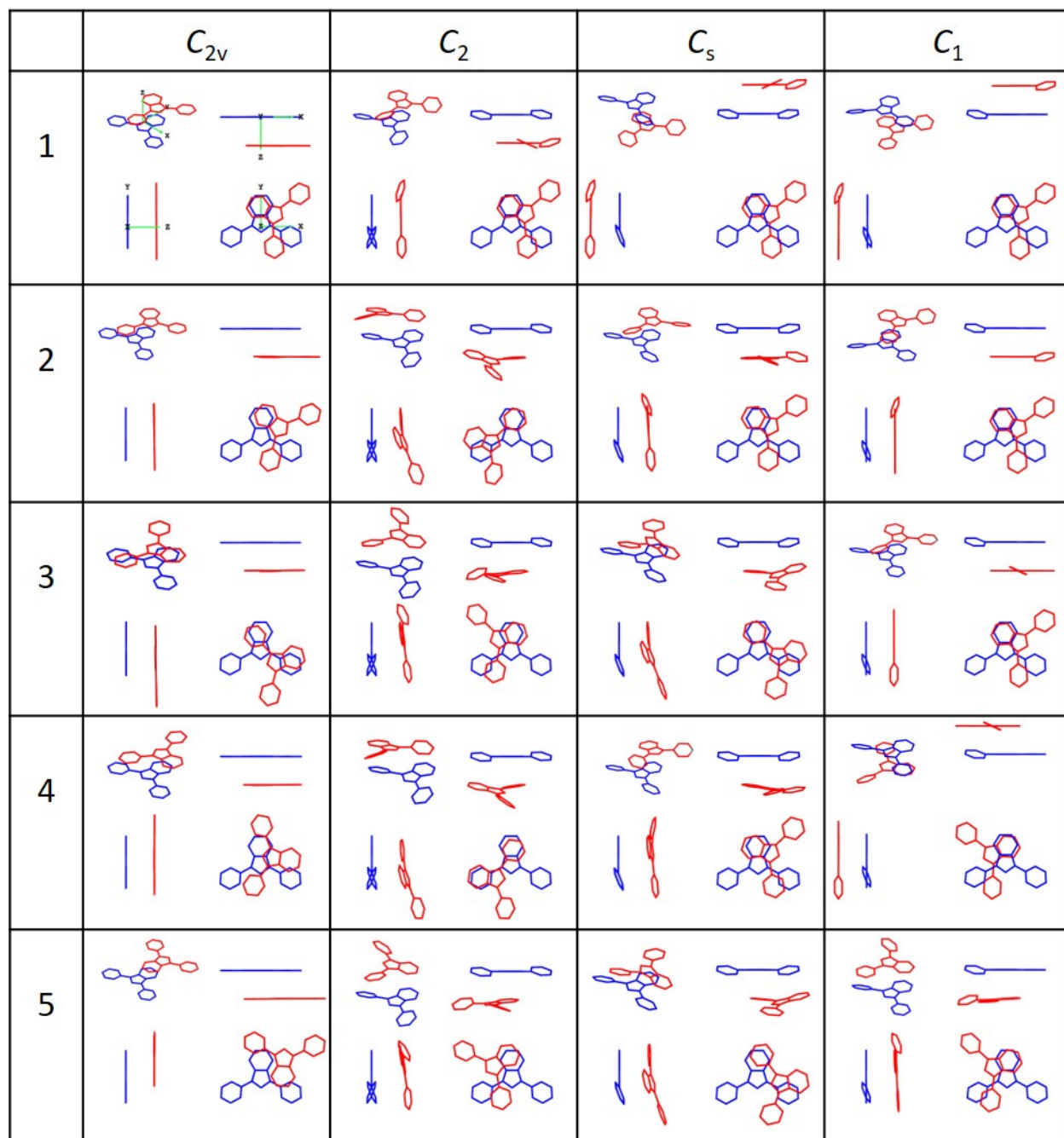


**Figure 4.** Multi-view projections of optimized pairs 1 through 5 for the four rotamers of **1**.

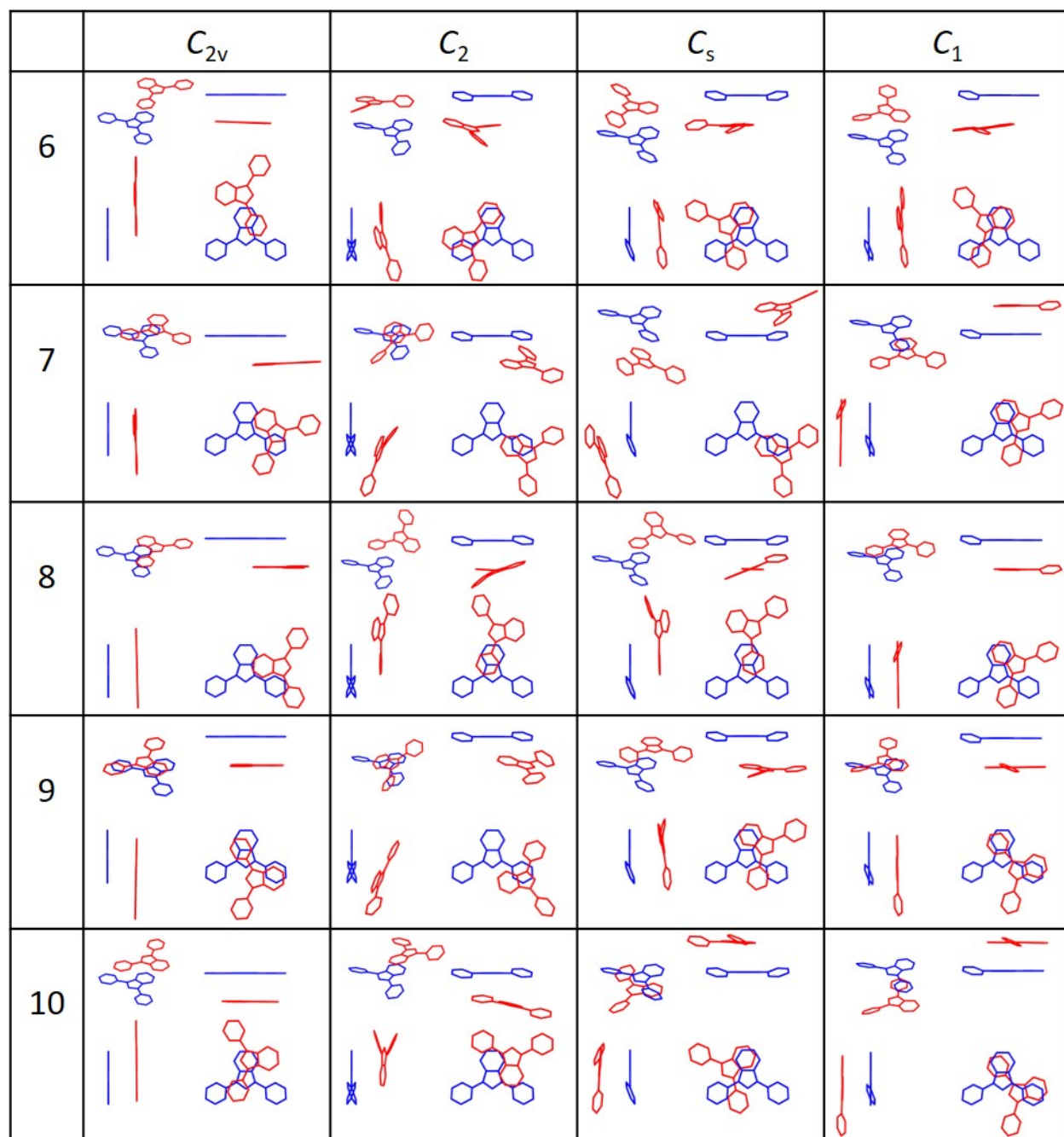


**Figure 5.** Multi-view projections of optimized pairs 5-10 for the four rotamers of **1**.

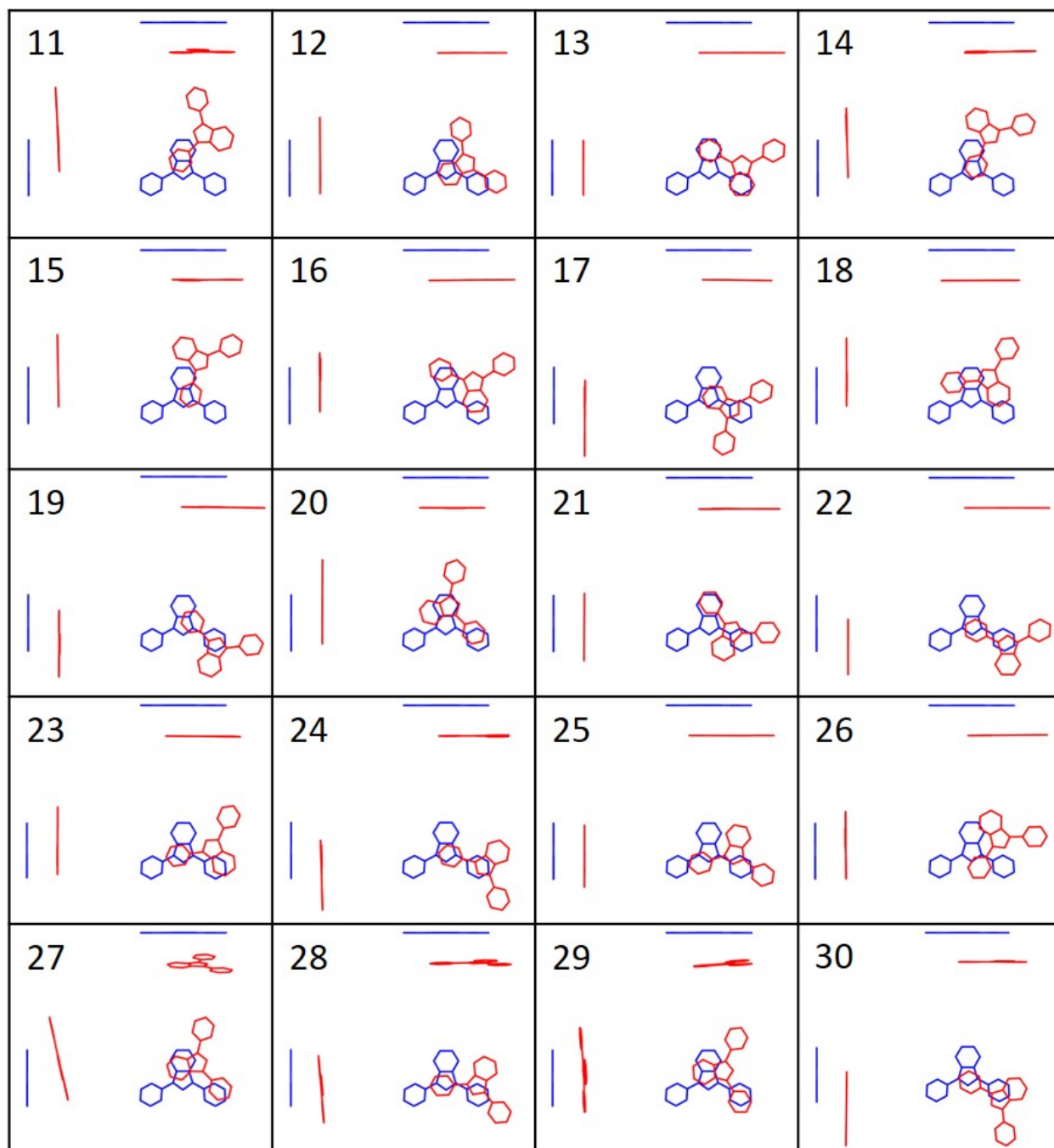


**Figure 6.** Multi-view projections of optimized pairs 11-30 for the  $C_{2v}$  rotamer of **1**.

**Table 1.** Calculated SF Energetics and Rate Constants for the Top 10 Pairs of **1(C<sub>2</sub>)**, **1(C<sub>s</sub>)**, and **1(C<sub>1</sub>)**.<sup>a</sup>

Struct.	$(h_A I_A   h_B I_B)$	$\Delta E_{DS}^b$	$ T^* ^2$	$\Delta E_{SF}(S^*)^c$	$ T^{**} ^2$	$\Delta E_{SF}(S^{**})^c$	$\Delta E_{BB}^d$	$k/k_0^e$
<b>C<sub>2</sub></b>								
1	5.8	51.3	1161.7	10.3	0.0	-41.0	34.7	4306
2	14.4	42.5	931.6	15.8	0.0	-26.6	37.6	2944
3	1.1	27.4	625.5	3.1	0.0	-24.4	24.6	2261
4	0.8	25.4	207.3	-5.9	8.7	-31.1	30.1	896
5	11.7	51.4	214.7	4.6	0.0	-46.8	26.8	892
6	5.2	4.3	141.3	-9.8	106.6	-14.1	29.0	806
7	1.6	5.4	149.9	-10.6	61.5	-16.1	23.6	717
8	0.5	9.3	132.5	-8.1	25.4	-17.4	20.8	546
9	1.7	3.4	123.8	-9.4	41.7	-12.8	20.3	536
10	34.2	334.9	334.9	58.7	3.3	-85.2	23.9	504
<b>C<sub>s</sub></b>								
1	11.4	70.5	1489.7	9.4	0.0	-61.1	45.9	5998
2	19.8	93.6	899.7	13.4	8.0	-80.2	46.2	3473
3	13.6	44.8	1022.2	18.2	0.0	-26.7	36.8	3126
4	2.9	32.2	511.5	6.6	0.5	-25.7	22.3	1805
5	1.9	15.3	179.8	-7.1	77.0	-22.4	29.5	901
6	16.1	63.4	185.6	4.7	2.9	-58.7	33.2	808
7	1.8	4.4	162.7	-10.1	68.5	-14.5	23.2	766
8	0.4	14.3	158.4	-5.9	51.3	-20.2	23.2	724
9	12.8	54.2	171.1	6.6	0.0	-47.6	25.6	691
10	19.6	80.7	167.6	15.1	0.0	-65.6	29.8	614
<b>C<sub>1</sub></b>								
1	12.9	76.1	3122.6	-19.7	0.0	-95.8	83.0	22252
2	14.6	83.0	2984.0	-15.9	0.0	-98.8	81.6	20037
3	15.3	87.1	2697.5	-9.4	0.3	-96.5	75.6	16130
4	18.1	99.5	2495.8	-1.7	0.0	-101.2	72.4	13025
5	3.6	49.3	1960.1	-2.6	0.0	-51.9	49.4	9267
6	2.5	42.0	1108.7	5.6	0.3	-36.4	33.1	4286
7	19.2	69.5	498.0	-14.0	0.0	-83.5	60.7	3148
8	21.9	78.3	486.3	-8.6	0.0	-86.9	60.4	2824
9	12.2	10.9	953.6	4.5	0.0	-6.4	42.5	2724
10	13.7	11.7	850.1	3.5	0.0	-8.2	43.5	2506

<sup>a</sup> Energies in units of meV and couplings in units of meV<sup>2</sup>. <sup>b</sup> Davydov splitting  $\Delta E_{SF} = E(S^{**}) - E(S^*)$ .

<sup>c</sup> Endoergicity of SF,  $\Delta E_{SF}(S^*) = E(^1TT^*) - E(S^*)$  and  $\Delta E_{SF}(S^{**}) = E(^1TT^*) - E(S^{**})$ .

<sup>d</sup> Biexciton binding energy. <sup>e</sup>  $k_0 = 1.05 \times 10^8 \text{ s}^{-1}$ .

**Table 2.** Calculated SF Energetics and Rate Constants for the Top 30 Pairs of **1**(C<sub>2v</sub>).<sup>a</sup>

Struct.	( $h_A I_A   h_B I_B$ )	$\Delta E_{DS}^b$	$ T^* ^2$	$\Delta E_{SF}(S^*)^c$	$ T^{**} ^2$	$\Delta E_{SF}(S^{**})^c$	$\Delta E_{BB}^d$	$k/k_0^e$
1	14.0	78.7	2628.9	-12.4	0.0	-91.1	75.3	16422
2	19.7	69.3	407.3	-7.5	0.0	-76.7	54.4	2273
3	10.0	8.2	742.3	7.1	0.0	-1.1	34.4	1927
4	3.4	16.1	386.0	-2.9	98.3	-19.0	27.8	1625
5	36.6	147.6	846.8	50.2	1.5	-97.4	42.7	1539
6	5.2	35.3	345.6	1.2	40.3	-34.1	28.0	1469
7	3.8	10.8	401.7	-6.2	3.4	-17.0	25.0	1419
8	22.7	96.2	376.5	33.1	49.9	-63.1	28.3	988
9	9.6	67.1	236.9	20.8	26.6	-46.2	28.3	772
10	6.7	34.3	168.8	-0.4	9.5	-34.6	23.1	714
11	10.2	34.7	130.6	9.9	93.3	-24.7	19.9	598
12	47.3	208.2	576.9	83.5	0.0	-124.7	30.2	494
13	14.5	79.8	237.5	45.4	0.0	-34.4	9.2	461
14	9.6	20.5	3.8	9.4	195.0	-11.1	11.8	398
15	2.5	5.4	136.8	1.8	1.9	-3.6	9.7	380
16	26.7	109.4	176.3	42.3	0.8	-67.1	19.9	377
17	41.9	176.8	251.9	64.8	0.0	-112.0	28.1	332
18	43.2	172.1	272.6	80.3	2.8	-91.9	19.9	252
19	3.0	12.4	47.9	4.3	44.7	-8.1	10.6	243
20	44.9	181.4	250.2	79.1	48.6	-102.2	23.7	238
21	44.3	157.8	218.7	74.0	58.1	-83.7	24.3	236
22	14.9	65.4	98.8	39.3	0.0	-26.2	6.3	212
23	19.5	77.5	80.1	32.0	11.2	-45.5	13.6	212
24	2.9	7.8	93.9	16.4	0.0	8.6	3.6	201
25	48.1	153.5	238.3	84.6	0.0	-68.9	22.4	198
26	6.4	18.1	0.1	2.8	84.1	-15.3	10.6	193
27	31.9	108.0	61.3	57.7	200.2	-50.4	14.6	132
28	25.1	100.1	62.2	47.7	0.0	-52.3	9.2	117
29	23.6	76.1	60.8	50.4	19.9	-25.7	6.8	113
30	5.6	24.2	22.1	14.5	29.6	-9.7	6.2	113

<sup>a</sup> Energies in units of meV and couplings in units of meV<sup>2</sup>. <sup>b</sup> Davydov splitting  $\Delta E_{SF} = E(S^{**}) - E(S^*)$ .

<sup>c</sup> Endoergicity of SF,  $\Delta E_{SF}(S^*) = E(^1TT^*) - E(S^*)$  and  $\Delta E_{SF}(S^{**}) = E(^1TT^*) - E(S^{**})$ .

<sup>d</sup> Biexciton binding energy. <sup>e</sup>  $k_0 = 1.05 \times 10^8 \text{ s}^{-1}$ .

It is evident from Figures 4 and 5 that the pair structures found for the  $C_2$ ,  $C_s$ , and  $C_1$  rotamers are all variations of pair structures found for the  $C_{2v}$  rotamer perturbed to accommodate the twisted phenyls.  $C_2$  pair 1 and 3,  $C_s$  pairs 1 and 2, and  $C_1$  pairs 1 through 6 are all of the same type as  $C_{2v}$  pair 1. As a result of the symmetry breaking due to the twisted phenyl rotamers, for every pair structure in the  $C_{2v}$  optimization there are multiple pairs in the  $C_2$ ,  $C_s$ , and  $C_1$  optimizations, where the arrangement of the isobenzofurans of partners A and B is very similar but the relative rotations of their phenyl groups differ. We will therefore primarily focus on results of the  $C_{2v}$  rotamer optimization for simplicity. Structures, energetics, and rate constant ratios for the top 67 optimized pair structures for each of the four rotamers are provided in the Supporting Information.

Multi-view projections of the slip-stacked crystal pair of **1** and the optimized pair structures which are most similar to it for each rotamer are shown in Figure 7 and energetics, couplings, and the SF rate constant ratios for these pairs are provided in Table 3.

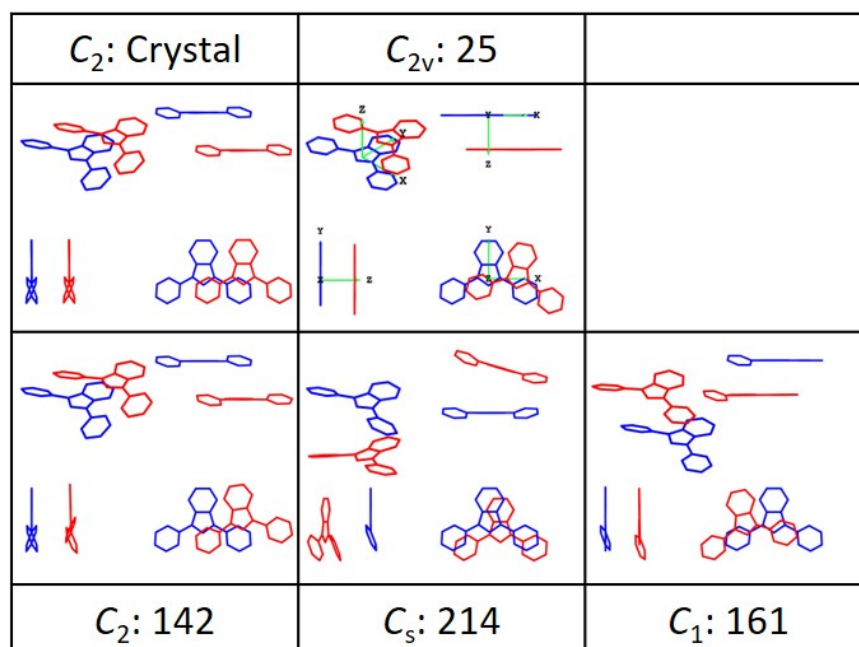


**Figure 7.** Multi-view projections of crystal pair and most similar optimized pairs for each rotamer.

**Table 3.** Calculated SF Energetics and Rate Constants for Crystal and Similar Pairs of **1**.<sup>a</sup>

Struct.	$(h_A l_A   h_B l_B)$	$\Delta E_{DS}^b$	$ T^* ^2$	$\Delta E_{SF}(S^*)^c$	$ T^{**} ^2$	$\Delta E_{SF}(S^{**})^c$	$\Delta E_{BB}^d$	$k/k_0^e$
Crystal <sup>f</sup>	19.0	72.7	0.4	36.2	0.0	-36.5	2.0	1.0
$C_2$ :142	19.5	77.8	0.4	38.0	0.0	-39.8	1.2	0.9
$C_{2v}$ :25	48.1	153.5	238.3	84.6	0.0	-68.9	22.4	198
$C_s$ :214	78.7	319.9	7.78	159.7	0.5	-160.3	3.1	1.0
$C_1$ :161	45.3	139.3	178.9	77.9	22.1	-61.3	21.3	175

<sup>a</sup> Energies in units of meV and couplings in units of meV<sup>2</sup>. <sup>b</sup> Davydov splitting  $\Delta E_{SF} = E(S^{**}) - E(S^*)$ .

<sup>c</sup> Endoergicity of SF,  $\Delta E_{SF}(S^*) = E(^1TT^*) - E(S^*)$  and  $\Delta E_{SF}(S^{**}) = E(^1TT^*) - E(S^{**})$ .

<sup>d</sup> Biexciton binding energy. <sup>e</sup>  $k_0 = 1.05 \times 10^8 \text{ s}^{-1}$ .

<sup>f</sup> Crystal slip-stacked pair structure in the  $\alpha$  form; the structure is nearly identical in the  $\beta$  form.

Of the 144 optimized pair structures of the  $C_2$  rotamer, the pair which most resembles the slip-stacked pair in the crystal is the 142nd. The primary differences between this structure and that in the crystal are an 8.3° rotation about the  $z$  axis and an additional 0.3 Å slip along the  $y$  axis for partner B. These modifications offer no improvement in SF rate constant. Of the optimized  $C_{2v}$  rotamer pairs, the most similar pair is 25. This pair's predicted rate constant is 198 times larger than that of the crystal pair. Pair 161 of the 291  $C_1$  rotamer pairs is very similar to pair 25 for the  $C_{2v}$  rotamer (they both have 11° rotation about the  $z$  axis and very similar translations) and consequently has a rate constant 175 times larger than that of the crystal pair. For the  $C_s$  rotamer, it is number 214 of 215 and it offers no improvement in SF rate constant. Despite a 20-fold increase in squared coupling over the crystal, this pair suffers from a large Davydov splitting of 320 meV and consequent endothermicity of SF of 160 meV from its  $S^*$  state.

The biexciton binding energy is an important factor in the evolution of the electronically and spin coupled  $^1TT^*$  state to the spatially separated  $^1(T...T)$  state that has lost electronic but not spin coherence. These values are reported in column 8 of Tables 1, 2, and 3, and most are below  $k_B T$  at

room temperature,  $\sim 26$  meV.  $C_{2v}$  pairs 1, 2, and 5 have relatively large binding energies of 75, 54, and 42 meV respectively, which may be cause for concern for these otherwise promising structures.

## Discussion

As stated above, we will mostly limit the discussion to  $C_{2v}$  optimized pairs but will note the strong effect that differences in the relative rotations of phenyl groups have on the predicted relative rates of SF. While pair 1 for each of the four rotamers is nearly identical in the arrangement of isobenzofurans, their different phenyl rotations result in 22 252 and 16 422 fold improvement of the SF rate constant for the  $C_1$  and  $C_{2v}$  rotamers but only 4 306 and 5 998 fold improvement for the  $C_2$  and  $C_s$  rotamers. The results make it clear that the two effects of intermolecular interactions, one on the coupling constant  $|T|$  and the other on the SF energy balance, are of comparable importance. At least in the case of **1**, the effect of intermolecular interactions on the biexciton binding energy is rarely significant.

$C_{2v}$  pairs 1 and 2 demonstrate the effect on the relative SF rate by small deviations from the optimized structure geometry. Partner B (in red in Figure 4) in pair 2 differs from its position in pair 1 by additional 0.09 and 0.56 Å slips along the  $x$  and  $y$  axes and is rotated  $16^\circ$  less about the  $z$  axis. These slight changes result in a relative rate of SF for pair 2 that is reduced by a staggering 73%. While the energetics remain similar, the squared coupling is reduced by 85%.

The SF energy balance is intimately tied to the magnitude of the Davydov splitting between the  $S^*$  and  $S^{**}$  states, which is mostly due to the interaction of the transition densities of partners A and B and only in part to the admixture of the CT configurations, as is clear from the comparison of numbers in columns 2 and 3. Boltzmann statistics favor SF from  $S^*$  and a large Davydov splitting

makes SF too endoergic, Indeed, the Davydov splitting for the top pair geometries is mostly below 100 meV. Favorable pair geometries also tend to have a large SF coupling to the S\* state and little or none to the S\*\* state when the Davydov splitting is significant e.g. pairs 1 through 3, 5, and 7. When the Davydov splitting is small, as in pairs 4, 6, and 11, the SF coupling tends to benefit from both S\* and S\*\*. Rarely is the coupling primarily to a slightly exothermic S\*\* state as found in pairs 14 and 26, and this only happens when the Davydov splitting is small and allows significant thermal population in S\*\*.

As also recognized by others,<sup>62</sup> a delicate compromise between the SF energy balance and the SF electronic matrix element thus must be struck in the optimization of pair geometries to maximize the predicted SF rate constant. Within the simplified model, one or both of the sums and differences of the overlaps in the pairs  $(S_{hh} - S_{ll})$  and  $(S_{hl} + S_{lh})$  or  $(S_{hh} + S_{ll})$  and  $(S_{hl} - S_{lh})$  must be large for large SF coupling (eqs. 4a and 4b); however, at the same time the interaction of the transition densities on partners A and B must not be excessive. This is achieved for **1** in two general classes of structures into which the majority of the optimized pair geometries fall.

One class comprises stacked pair structures with overlapping aromatic rings such as pairs 1, 2, 3, 9, and 13. These pairs can overlap their benzene units (pairs 1 and 2) and then rotate partner B to reduce excitonic splitting and achieve a very large SF coupling. Pair 1 has a squared coupling and improved rate which dwarf all others at 2629 meV<sup>2</sup> and 16 422 fold, respectively, while a very slight translation and rotation results in pair 2 having about one sixth the coupling squared and one seventh the rate improvement. This massive increase in SF rate constant requires at least one phenyl in plane with the isobenzofuran and is accordingly only present in the top C<sub>2v</sub> and C<sub>1</sub> structures. Pairs 3, 9, and 13 are examples where the benzene unit of partner A overlaps a phenyl of B and the

benzene unit of B overlaps a phenyl of A. About half of each molecule has overlap with its partner but the other half does not. The result of these structures are 1 927, 722, and 461 fold rate improvements of for pairs 3, 9, and 13.

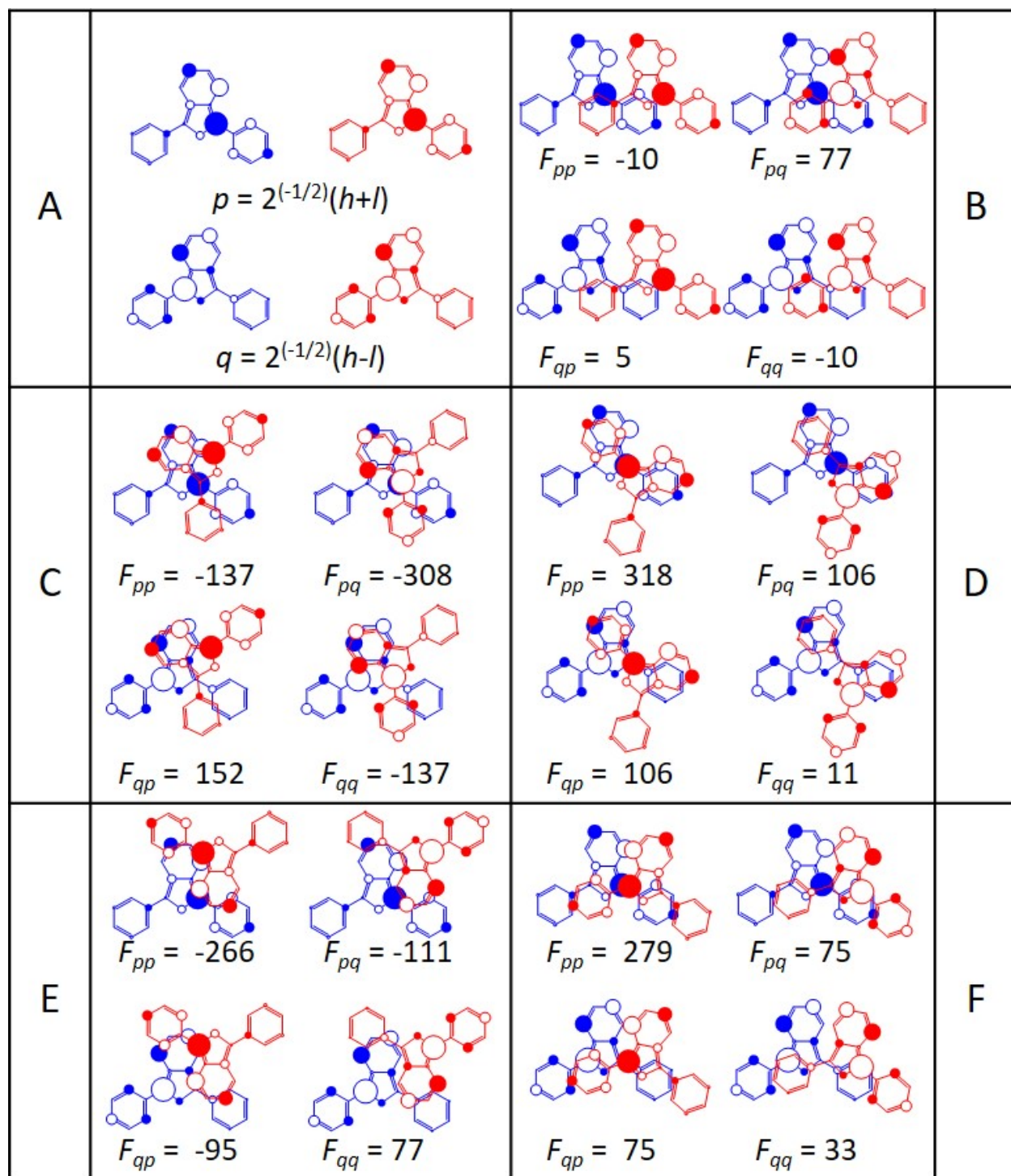


**Figure 8.** a) Semi-localized orbitals  $p$  and  $q$  for the qualitative analysis of b) slip-stacked crystal pair and  $C_{2v}$  optimized pairs C: 1, D: 3, E: 5, and F: 25. Approximate values of the Fock matrix elements between semi-localized orbitals are provided.

Figure 8 shows the semi-localized orbitals  $p = 2^{-1/2}(h + l)$  and  $q = 2^{-1/2}(h - l)$  where  $h$  and  $l$  are the HOMO and LUMO. The SF matrix element is related to the overlaps  $S_{pp}$ ,  $S_{pa}$ ,  $S_{qp}$ , and  $S_{qq}$  (eqs. 4a and 4b). The overlaps and the SF matrix elements can be visually estimated in panels B through F of Figure 8. For pair 1, one can easily see the large negative values for the overlaps  $S_{pp}$  and  $S_{pq}$  and the large positive value for  $S_{qp}$ . The value of  $S_{qq}$  is small and negative, resulting in a very large value for  $|T|$  and zero for  $|T^+|$ . Pair 3 has a large positive value for  $S_{pp}$  and a small positive value for  $S_{pq}$ , but moderate values for  $S_{qp}$  and  $S_{qq}$  with the opposite sign, again resulting in a large value for  $|T|$  and zero for  $|T^+|$ .

The other major class of optimized pairs comprises those with overlapping perimeters. Some examples are pairs 4, 5, 6, 8, and 25. Pair 5 has double the squared coupling of pairs 4 and 6, but is much more endothermic, reducing its potential enhancement of the SF rate constant. These five pairs have rate constants enhanced 1 625, 1 539, 1 469, 988, and 198 fold. Looking at the semi-localized orbital overlaps in Figure 8 it is easy to understand why these structures are favorable. For pair 6, there is very large negative orbital overlap between  $p_A$  and  $p_B$ . The orbitals  $q_A$  and  $p_B$  have large negative overlap while  $p_A$  and  $q_B$  have medium negative overlap. The overlap of  $q_A$  and  $q_B$  is small and positive, resulting in a large coupling  $|T|$ . Overlapping the perimeters allows pair 6 to have a good SF coupling of 345 meV<sup>2</sup> and minimal excitonic stabilization, with SF being only 1.2 meV endothermic. This is because overlapping just the perimeter allows the majority of the singlet transition charge densities on partners A and B to be far away from each other, greatly reducing their interaction (eqs. 4c-f).

The qualitative rules and semi-local orbitals also explain why pair 25 is predicted to have a SF rate constant 198 times larger than that of the crystal pair though they are similar. In the slip-

stacked crystal pair, partner B is rotated and translated towards A such that the large orbital coefficient on the carbon in the furan ring to which one phenyl is attached has very large overlap with the same atomic orbital on its partner. The decreased separation between the partners in 25 has the effect of doubling the Davydov splitting and endoergicity; however this is more than compensated by the 600-fold increase in coupling squared. This again demonstrates the importance of balancing SF coupling and energetics.

## Conclusion

The results of the optimizations of pairs of four rotamers of 1,3-diphenylisobenzofuran with  $C_2$ ,  $C_{2v}$ ,  $C_s$ , and  $C_1$  symmetry resulted in 142, 67, 214, and 291 pair structures with singlet fission rate constants predicted to be larger than that found in its regular crystal form. While the simple nature of the model limits its accuracy, certainly many of the top structures predicted are good targets for synthetic efforts and promise large increases in the rates of singlet fission. Structural motifs which overlap sections of the two partners or their perimeters appear to be ideal. None of these structures seem to have been reported in the literature but their synthesis appears feasible, either by crystal engineering or by preparation of covalent dimers. The predicted SF rate constants are sensitive to relatively small deviations in the relative orientations of the optimized pairs, demonstrated by pairs 1 and 2 for the  $C_{2v}$  rotamer, likely making the synthesis all the more challenging.

**Acknowledgment.** This work was supported by the U.S. Department of Energy, Office of Basic Energy Sciences, Division of Chemical Sciences, Biosciences, and Geosciences, under award number DE-SC0007004. Geometry optimizations utilized the RMACC Summit<sup>63</sup> supercomputer,

which is supported by the National Science Foundation (awards ACI-1532235 and ACI-1532236), the University of Colorado Boulder, and Colorado State University. The Summit supercomputer is a joint effort of the University of Colorado Boulder and Colorado State University.

## References

1. M. B. Smith and J. Michl, *Chem. Rev.*, 2010, **110**, 6891.
2. M. B. Smith and J. Michl, *Annu. Rev. Phys. Chem.*, 2013, **64**, 361.
3. D. Casanova, *Chem. Rev.*, 2018, **118**, 7164.
4. K. Miyata, F. S. Conrad-Burton, F. L. Geyer and X.-Y. Zhu, *Chem. Rev.*, 2019, **119**, 4261.
5. M. C. Hanna and A. J. Nozik, *J. App. Phys.*, 2006, **100**, 074510.
6. W. Shockley and H. J. Queisser, *J. App. Phys.*, 1961, **32**, 510.
7. W. G. Albrecht, M. E. Michel-Beyerle and V. Yakhot, *Chem. Phys.*, 1978, **35**, 193.
8. R. J. Dillon, G. B. Piland, and C. J. Bardeen, *J. Am. Chem. Soc.*, 2013, **135**, 17278.
9. J. L. Ryerson, J. N. Schrauben, A. J. Ferguson, S. C. Sahoo, P. Naumov, Z. Havlas, J. Michl, A. J. Nozik and J. C. Johnson, *J. Phys. Chem. C*, 2014, **118**, 12121.
10. D. H. Arias, J. L. Ryerson, J. D. Cook, N. H. Damrauer and J. C. Johnson, *Chem. Sci.*, 2016, **7.2**, 1185.
11. S. T. Roberts, R. E. McAnally, J. N. Mastron, D. H. Webber, M. T. Whited, R. L. Brutchey, M. E. Thompson and S. E. Bradforth, *J. Am. Chem. Soc.*, 2012, **134**, 6388.
12. P. I. Dron, J. Michl and J. C. Johnson, *J. Phys. Chem. A*, 2017, **121**, 8596.
13. S. R. Yost, J. Lee, M. W. B. Wilson, T. Wu, D. P. McMahon, R. R. Parkhurst, N. J. Thompson, D. N. Congreve, A. Rao, K. Johnson and M. Y. A. Sfeir, *Nat. Chem.*, 2014, **6**,

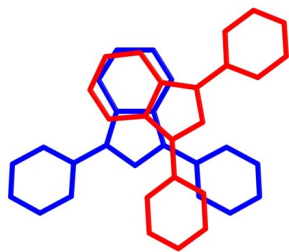
- 492.
14. S. W. Eaton, S. A. Miller, E. A. Margulies, L. E. Shoer, R. D. Schaller and M. R. Wasielewski, *J. Phys. Chem. A*, 2015, **119**, 4151.
  15. J. C. Johnson and A. J. Nozik, *Acc. Chem. Res.*, 2013, **46**, 1290.
  16. Y. J. Bae, G. Kang, C. D. Malliakas, J. N. Nelson, J. Zhou, R. M. Young, Y.-L. Wu, R. P. Van Duyne, G. C. Schatz and M. R. Wasielewski, *J. Am. Chem. Soc.*, 2018, **140**, 15140.
  17. W. L. Chan, T. C. Berkelbach, M. R. Provorse, N. R. Monahan, J. R. Tritsch, M. S. Hybertsen, D. R. Reichman, J. Gao and X. Y. Zhu, *Acc. Chem. Res.*, 2013, **46**, 1321.
  18. H. Zang, Y. Ke, Y. Zhao and W. Liang, *J. Phys. Chem. C*, 2016, **120**, 13351.
  19. J. E. Elenewski, U. S. Cubeta, E. Ko and H. Chen, *J. Phys. Chem. C*, 2017, **121**, 4130.
  20. S. Ito, T. Nagami and M. Nakano, *Phys. Chem. Chem. Phys.*, 2017, **19**, 5737.
  21. M. Nakano, K. Okada, T. Nagami, T. Tonami, R. Kishi and Y. Kitagawa, *Molecules*, 2019, **24**, 541.
  22. E. A. Buchanan, J. Kaleta, J. Wen, S. H. Lapidus, I. Čísařová, Z. Havlas, J. C. Johnson and J. Michl, *J. Phys. Chem. Lett.*, 2019, **10**, 1947.
  23. J. C. Johnson, A. J. Nozik and J. Michl, *J. Am. Chem. Soc.*, 2010, **132**, 16302.
  24. J. C. Johnson and J. Michl, *Top. Curr. Chem.*, 2017, **375**, 80.
  25. J. C. Johnson and J. Michl, in *Advanced Concepts in Photovoltaics*, eds. A. J. Nozik, G. Conibeer and M. C. Beard, Royal Society of Chemistry, Oxfordshire, UK, 2014, p. 324.
  26. J. Schrauben, J. Ryerson, J. Michl and J. Johnson, *J. Am. Chem. Soc.*, 2014, **136**, 7363.
  27. A. F. Schwerin, J. C. Johnson, M. B. Smith, P. Sreearunothai, D. Popović, J. Černý, Z. Havlas, I. Paci, A. Akdag, M. K. MacLeod, X. Chen, D. E. David, M. A. Ratner, J. R. Miller, A. J. Nozik and J. Michl, *J. Phys. Chem. A*, 2010, **114**, 1457.

28. I. Paci, J. C. Johnson, X. Chen, G. Rana, D. Popović, D. E. David, A. J. Nozik, M. A. Ratner and J. Michl, *J. Am. Chem. Soc.*, 2006, **128**, 16546.
29. J. Kaleta, E. A. Buchanan, M. Tan, I. Císařová, B. Kahr, J. C. Johnson and J. Michl, unpublished results.
30. A. Zaykov, P. Felkel, E. A. Buchanan, M. Jovanovic, R. W. A. Havenith, R. K. Kathir, R. Broer, Z. Havlas and J. Michl, unpublished results.
31. R. A. Marcus, *Rev. Mod. Phys.*, 1993, **65**, 599.
32. R. A. Marcus, *J. Chem. Phys.*, 1956, **24**, 966 and 979.
33. R. A. Marcus, *Biochim. Biophys. Acta*, 1985, **811**, 265.
34. J. L. Ryerson, A. Zaykov, R. W. A. Havenith, L. E. Aguilar Suarez, S. Faraji, B. R. Stepp, A. Wahab, P. I. Dron, J. Kaleta, S. J. Teat, J. Ludvík, J. R. Miller, Z. Havlas, R. Broer, J. Michl and J. C. Johnson, unpublished results.
35. E. A. Buchanan, Z. Havlas and J. Michl, in *Advances in Quantum Chemistry: Ratner Volume, 75*, eds. J. R. Sabin and E. J. Brändas, Elsevier, Cambridge, MA, 2017, p. 175.
36. E. A. Buchanan, Z. Havlas and J. Michl, unpublished results.
37. E. A. Buchanan and J. Michl, *J. Am. Chem. Soc.*, 2017, **139**, 15572.
38. K. A. Král, *Czech J. Phys. B*, 1972, **22**, 566.
39. J. Jortner, S. A. Rice, J. L. Katz, S.-I. Choi, *J. Chem. Phys.* 1965, **42**, 309.
40. W. G. Herkstroeter and P. B. Merkel, *J. Photochem.*, 1981, **16**, 331.
41. J. C. Johnson, A. Akdag, M. Zamadar, X. Chen, A. F. Schwerin, I. Paci, M. B. Smith, Z. Havlas, J. R. Miller, M. A. Ratner, A. J. Nozik and J. Michl, *J. Phys. Chem. B*, 2013, **117**, 4680.

42. I. Fischer-Hjalmars, *J. Chem. Phys.*, 1965, **42**, 1962.
43. M. Wolfsberg and L. Helmholz, *J. Chem. Phys.*, 1952, **20**, 837.
44. R. Hoffmann, *J. Chem. Phys.*, 1963, **39**, 1397.
45. J. Linderberg and L. Seamans, *Mol. Phys.*, 1972, **24**, 1393.
46. S. Harris, *An Introduction to the Theory of the Boltzmann Equation*, Holt, Rinehart and Winston, New York, 1971.
47. J. E. Subotnik, J. Vura-Weis, A. J. Sodt and M. A. Ratner, *J. Phys. Chem. A*, 2010, **114**, 8665.
48. F. Neese, *Wiley Interdiscip. Rev.: Comput. Mol. Sci.*, 2012, **2**, 73.
49. S. Hirata and M. Head-Gordon, *Chem. Phys. Lett.*, 1999, **314**, 291.
50. C. Adamo and V. Barone, *J. Chem. Phys.*, 1999, **110**, 6158.
51. F. Weigend and R. Ahlrichs, *Phys. Chem. Chem. Phys.*, 2005, **7**, 3297.
52. R. Izsak and F. Neese, *J. Chem. Phys.*, 2011, **135**, 144105.
53. F. Neese, F. Wennmohs, A. Hansen and U. Becker, *Chem. Phys.*, 2009, **356**, 98.
54. F. Weigend, *J. Comput. Chem.*, 2008, **29**, 167.
55. D. Rappoport and F. Furche, *J. Chem. Phys.* 2010, **133**, 134105.
56. G. L. Stoychev, A. A. Auer, and F. Neese, *J. Chem. Theory Comput.*, 2017, **13**, 554.
57. E. K. U. Gross and W. Kohn, *Adv. Quantum Chem.*, 1990, **21**, 255.
58. R. O. Jones and O. Gunnarsson, *Rev. Mod. Phys.*, 1989, **61**, 689.
59. C. C. J. Roothaan, L. M. Sachs and A. W. Weiss, *Rev. Mod. Phys.*, 1960, **32**, 186.
60. R. Krishnan, J. S. Binkley, R. Seeger and J. A. Pople, *J. Chem. Phys.*, 1980, **72**, 650.
61. E. D. Glendening, C. R. Landis and F. Weinhold, *J. Comput. Chem.*, 2013, **34**, 1429.
62. A. K. Le, J. A. Bender, D. H. Arias, D. E. Cotton. J. C. Johnson and S. T. Roberts, *J. Am.*

*Chem. Soc.*, 2018, **140**, 814.

63. J. Anderson, P. J. Burns, D. Milroy, P. Ruprecht, T. Hauser and H. J. Siegel, in *Proceedings of the Practice and Experience in Advanced Research Computing 2017 on Sustainability, Success and Impact*, July 09-13, 2017, New Orleans, LA, USA. DOI: 10.1145/3093338.3093379



Best molecular pair packing geometries for singlet fission in 1,3-diphenylisobenzofuran are predicted.